High Performance Elastomeric Nanocomposites via Solvent Exchange Processing

Shawna M. Liff, Nitin Kumar, Gareth H. McKinley*

Institute for Soldier Nanotechnologies and Department of Mechanical Engineering

Massachusetts Institute of Technology

77 Massachusetts Ave, NE47-511

Cambridge, Massachusetts 02139

Correspondence should be addressed to GHM

*: gareth@mit.edu

Ph: (617) 258-0754

Abstract

The incorporation of nanoparticles into engineering thermoplastics affords engineers an opportunity to synthesize polymer nanocomposites that potentially rival the most advanced materials in nature. Development of these materials is difficult since thermodynamic and kinetic barriers inhibit the dispersal of inorganic, often hydrophilic nanoparticles in hydrophobic polymer matrices. Using a new solvent exchange approach we preferentially nanoreinforce the hard micro-domains of thermoplastic elastomers with smectic clay of similar characteristic dimensions. The strong adhesion between the clay and the hard micro-domains coupled with the formation of a percolative network not only stiffens and toughens, but increases the heat distortion temperature of the material and induces reversible thermotropic liquid-crystalline transitions. The discotic clay platelets induce morphological ordering over a range of length scales that results in significant thermomechanical enhancement and expands high temperature applications. Merging block-copolymer processing techniques with this method for nanoparticle preferential-ordering facilitates the development of new, hierarchically-ordered materials.

Text

High performance biomaterials, such as silk[1-5] and bone[6, 7] exhibit unparalleled combinations of stiffness, strength, extensibility, and toughness by exploiting hierarchical structures in which stiff nanometer-size crystallites are embedded and dispersed in softer protein matrices[1-3, 8]. Polymer nanocomposites which utilize engineering thermoplastics as the matrix material and stiff, inorganic, anisotropic nanoparticles to tailor thermomechanical properties have been the subject of many recent studies[9, 10]. Successful mechanical enhancement of polymer matrices via nanoreinforcement is expected only when the nanoparticles are fully exfoliated in

the polymer matrix. This is difficult since the organic, hydrophobic polymer matrices thermodynamically and kinetically inhibit the dispersal of the inorganic, hydrophilic clay. Despite numerous advances synthetic polymer nanocomposites have yet to display the superior toughness of natural biomaterials, such as silk. Like a majority of engineering materials the nanocomposites are either stiff but not extensible, like steel, or extensible but not stiff, like rubber. In the present work we outline a novel solvent exchange approach to efficiently exfoliate nanoparticles, particularly synthetic smectic clays, such as Laponite® RD, in commercial thermoplastic polyurethane (TPU) elastomers, such as Elasthane^{TM} 80A.

Elasthane, an elastomeric block-copolymer, is composed of hard segments (HS) and soft segments (SS) which combine to give the TPU moderate stiffness, high rubber-like extensibility, and easy processibility[11, 12] (**Fig. 1a**). Thermodynamic incompatibility of the HS and SS drives the polymer system into a two-phase morphology in which hydrogen-bonded, crystalline hard micro-domains form amid the rubbery soft domains. Depending on the specific segmental composition and the interaction between soft and hard segments, the hard micro-domains can form fibrillar, globular, or lamellar structures within a continuous soft matrix or form an interconnected hard domain network[13, 14]. Because the polyurethane HS has a high melting temperature ($T_{m,HS} > T_{room}$) and the SS has a low glass transition temperature ($T_{g,SS} < T_{room}$), at room temperatures the hard and soft domains are in crystalline and rubbery states, respectively. The stiffness (or elastic modulus, E) and strength (tensile stress at break, σ_{max}) of the TPU increases with HS content while the extensibility (strain at failure, ε_{max}) increases with SS content[15-19]. The flexibility of urethane chemistry enables the chemical structure of the HS and SS domains to be varied to control the thermal transition temperatures and thermomechanical properties of the polyurethane[20, 21]. Synthetically it is difficult to increase the elastic modulus of a

polyurethane and maintain its high extensibility, or vice-versa—an increase in one often results in a decrease in the other[11].

Recent studies of high performance biomaterials such as spider silk show that araneid spiders modify the stiffness and strength of silk by regulating ordering of polypeptide chains and/or through formation of nano-crystallites during spinning[22, 23]. Following previous polymer nanocomposite work[9, 10, 24, 25], we thus chose to stiffen and strengthen a commercial synthetic TPU with low aspect-ratio clay platelets. Very recently, Finnigan et al. have studied a similar TPU (but with higher soft segment weight fraction and with a spherical morphology) filled with a single weight fraction of clay (3 wt%)[13]. They show that the aspect-ratio of the silicates modifies the mechanical behavior but does not change the phase morphology. To increase E and σ_{max} of Elasthane while maintaining its high ε_{max}, it is necessary to preferentially nanoreinforce the polyurethane hard micro-domains with unmodified Laponite nanoparticles. The stronger affinity of the hydrophilic, non-surface-modified Laponite with the more polar HS rather than with the SS allows the Laponite to segregate into the hard micro-domains during the processing of the TPU. By preferentially restricting the Laponite particles to the hard micro-domains the undesired stiffening of the soft domain is avoided and the large ε_{max} of the polyurethane composite remains uncompromised. To optimize this micro-segregation it is key that the dimension of the discotic clay platelets is similar in magnitude to the natural dimensions of the HS domains that microphase separate (HS length = 3-11 nm[19, 26], **Fig. 1a**). Consequently, Laponite (diameter, d = 25 nm, thickness l = 1 nm, aspect-ratio $\alpha = d / l = 25$) is more suitable for the preferential nanoreinforcement of the hard micro-domains than other high aspect-ratio clays (*e.g.* Montmorillonite and Hectorite with d=100-300 nm[24]) that are commonly used in polymer nanocomposites.

Full exfoliation of smectic clay particles in polymers is a major challenge. In the dry form smectic clays exist as agglomerates of stacked platelets tightly bound to each other via strong ionic and van der Waals forces. The current methods to exfoliate clay particles in engineering thermoplastics have been only partially successful; specifically, exfoliation in high molecular weight, strongly hydrophobic polymers that are insoluble in aqueous solution has proven to be particularly difficult[24, 27]. Typical methods[28] include (i) melt extrusion of unmodified and organically modified clay and (ii) dispersion of organically modified clay in organic solvent followed by in-situ polymerization[29] or dissolution of the matrix polymer and solvent casting. Organic modification of the clay surface has been found to be necessary to increase the affinity of clay with hydrophobic polymers or organic solvents; however, disadvantages such as premature degradation of the polymer and/or decreased thermomechanical properties have been reported[30]. Even with organic modification, good exfoliation remains a challenge[30-32].

To exploit the affinity of unmodified Laponite for the polar hard micro-domains of the Elasthane, a dispersal technique that does not rely upon chemical modification is necessary. Laponite powder can be dispersed in many organic, polar solvents due to its hydrophilic character which promotes the separation of clay platelets via osmotic pressure produced by the hydration of intercalated ions[29]. In non-polar solvents, the large energy barrier created by the reduced wettability and the absence of osmotically driven platelet separation prevents direct dispersion of Laponite. A novel solvent exchange method[33] was developed to disperse polar nanoparticles, such as Laponite, in organic solvents. This procedure requires the use of two solvents, A and B that meet four criteria; (i) solvent A must fully disperse the hydrophilic clay, (ii) solvent B must dissolve the polymer matrix and not cause re-aggregation of the nano-clay, (iii) solvents A and B must be fully miscible, and (iv) solvent B must have a higher boiling point

than solvent A. Solvents with high dipole moments and dielectric constants were found to be the most suitable B solvents. For this study, the chosen solvent pair was deionized water (DI; A) and dimethylacetamide (DMAc; B). Fully exfoliated dispersions of Laponite in DMAc were prepared following the solvent exchange approach[33] and Elasthane/Laponite thin films containing between 0 and 20 wt% Laponite were slowly solution cast for thermomechanical characterization (Methods).

The efficacy of the solvent exchange approach for exfoliating the Laponite is demonstrated in the TEM micrographs, AFM phase images, and WAXD data shown in **Figs. 1b-f**, **S1** & **S2**. The TEM images show exfoliated and randomly oriented single Laponite platelets. As the Laponite concentration, ϕ, exceeds the percolation threshold, $\phi_P \approx 5.9$ wt% (or $\tilde{\phi}_P \approx 2.5$ vol%), particle-particle interactions necessarily become important during the slow solvent evaporation and the instances of intercalated platelets with a spacing of 2 nm, however infrequent, increase. The percolation threshold, ϕ_P, represents the concentration at which the average inter-particle spacing is less than one particle diameter.

Because Laponite preferentially reinforces the hard micro-domains of Elasthane and concentrations greater than 5.9 wt% induce jamming, the influence on the mechanical properties of Elasthane is profound. The tensile curve of pure Elasthane (ϕ = 0 wt%) shown in **Fig. 2a** is similar to that of other TPUs[34, 35] in which three distinguishable deformation regions are readily identified. The first region where the stress, σ, increases linearly with strain, ε, is a region of elastic deformation and is governed by TPU crystallinity, hard segment content and ordering[35]. Yield corresponds to break-up of an interconnected hard domain network and is followed by two distinct regions of plastic deformation[14, 35]. The region of moderate slope is indicative of soft domain deformation plus rotation and alignment of the smaller hard micro-domains. The last

region characterized by the steep upturn in the σ-ε curve corresponds to the stretching and strain-induced crystallization of the soft-segments as well as further break-up of the hard micro-domains[14]. The addition of Laponite significantly increases the initial modulus of the material and the magnitude of the plateau and ultimate stress, but does not affect the slope due to soft segment stretching after yield or slope due to soft-segment strain-induced crystallization or hardening. However, the onset of plastic deformation and strain-hardening both occur at smaller deformations with increasing Laponite concentration.

The dramatic impact of Laponite on the elastic modulus of the polyurethane is shown in **Figs. 2a-c**. The modulus, *E,* increases with increasing Laponite concentration from 38 MPa at $\phi = 0$ wt% to 70.5 MPa at $\phi = 4$ wt% to 856 MPa at $\phi = 20$ wt%. This 23-fold increase in modulus, and specifically the sharp increase in E at $\phi \geq 6$ wt%, is a consequence of the percolative Laponite network. Below ϕ_P the platelets are randomly dispersed with an average inter-particle spacing greater than one particle diameter. Above ϕ_P, the Laponite forms a jammed structure which significantly hinders the mobility of hard and soft micro-domains during imposed deformation. Note the nanocomposites containing 15 and 20 wt% Laponite exhibit a sudden decrease in σ after yield, a behavior typical of glassy polymers[36]. This result corresponds to the sudden collapse of the jammed structure at which point the yield stress exceeds the stress that can be supported by the soft domains without significant reorientation and alignment.

The increase in E below the percolation limit can be modeled by Guth's equation[37] which was extended for anisotropic particles:

$$E = E_0(1 + 0.67\alpha\tilde{\phi} + 1.62\alpha^2\tilde{\phi}^2), \quad \text{for } \tilde{\phi} < \tilde{\phi}_P \tag{1}$$

Above the percolation limit, a power law scaling typical of jammed systems, such as gels[38] and glasses[39], is observed:

$$E = E_1 + A(\tilde{\phi} - \tilde{\phi}_P)^n \quad \text{for } \tilde{\phi} > \tilde{\phi}_P \tag{2}$$

where $\tilde{\phi}$ is the volume fraction of Laponite, $\tilde{\phi}_P$ is the percolation threshold volume fraction of Laponite, E_0 is the elastic modulus of pure Elasthane, and A and n are model parameters. The predicted values of E using Eq. 1 with E_0 = 38 MPa and α = 25 agree with experimental data. The aspect ratio, α = 25, of a single Laponite platelet further indicates that the Laponite platelets are fully exfoliated. Above the percolation threshold Eq. 2 is used with $\{E_1, A, n\}$ = {110 MPa, 1.54x10^5 MPa, 2}. The scaling factor, n, depends on numerous system properties including particle size, shape, polydispersity, and the particle-particle interaction potential[38, 39]. As shown in Fig. 2c the toughness at ε = 0.3 increases quadratically with $\tilde{\phi}$ in a manner similar to the Guth prediction for modulus. Thus

$$U_{0.3} = U_{0.3}^0\left(1 + 0.415\alpha\tilde{\phi} + 0.345\alpha^2\tilde{\phi}^2\right) \tag{3}$$

where $U_{0.3}^0$ = 0.916 MJ.m^{-3} and $U_{0.3}$ increases from 0.86 MJ.m^{-3} at ϕ = 0 wt% to 3.7 MJ.m^{-3} at ϕ = 20 wt%.

The impact of Laponite concentration on the extensibility (ε_{max}), strength (σ_{max}), and overall toughness (U_{max}) is not as dramatic. There is no significant change in the extensibility (ε_{max}) of Elasthane with Laponite—all nanocomposites exhibit ε_{max} = 4.23 ± 0.4. This suggests that the ultimate extensibility of the elastic network of soft domains is not compromised by reinforcing the hard domains. Both σ_{max} and U_{max} increase when Laponite is added to Elasthane.

In comparison, other elastomeric nanocomposites reinforced with either smectic clays [30-32, 40], carbon nanotubes [41], or fullerene[42] have only exhibited up to a six-fold increase in E and these enhancements are often accompanied by reductions in either ε_{max}, σ_{max}, or both. In the Elasthane/Laponite nanocomposite, the ultimate tensile strength σ_{max} plateaus at ϕ = 10 wt%, exhibiting a 50% increase from 32 MPa at ϕ = 0 wt% to 50 MPa at ϕ = 10 wt%. Similarly, U_{max} plateaus at ϕ = 15 wt% and exhibits a 100% increase, raising U_{max} from 48 MJ.m^{-3} at ϕ = 0 wt% to 95 MJ.m^{-3} at ϕ = 15 wt%. The Laponite toughens the Elasthane matrix in a manner similar to that in which hard, crystalline, mineral platelets toughen bone and nacre[6, 43]. The successful toughening of the Elasthane with Laponite is a result of the strong affinity, and thereby strong interfacial adhesion, of the Laponite with the polyurethane hard domain.

The 23-fold increase in E and increase in σ_{max}, $U_{0.3}$ and U_{max} without a concomitant reduction in ε_{max}, and without a change in the slope of the tensile curve during strain-hardening results because the Laponite is preferentially embedded within the polyurethane hard micro-domains rather than in the soft domain and drives interconnections between the hard micro-domains as observed with AFM (**Fig. S2**). As shown in **Fig. 3a** and **Fig. S3** the insignificant change in the soft segment glass transition temperature, $T_{g,SS}$, combined with the large increase in heat distortion temperature (HDT) and large increase in the magnitude of the flexural storage modulus, $E'(\phi, T)$, for temperatures $T > T_{g,SS}$, confirms that Laponite platelets are preferentially embedded in the hard micro-domains. Only at $\phi \geq$ 15 wt% does Laponite begin to observably enter the soft domains of the Elasthane and induce soft segment crystallinity.

In addition to identifying the location of preferential nanoreinforcement, the dynamic mechanical analysis (DMA) data for the various nanocomposites depicted in **Fig. 3b** elucidates the influence of Laponite concentration on the flexural storage modulus, $E'(\phi, T)$. The

magnitude of the rubbery plateau modulus at 25°C scales like the elastic modulus, E, and exhibits a 25-fold enhancement from $E' = 24$ MPa at $\phi = 0$ wt% to $E' = 600$ MPa at $\phi = 20$ wt%. Again, this enhancement is due to the percolative network established by the exfoliated Laponite platelets which are preferentially embedded within the TPU hard micro-domains. Consequently, the addition of Laponite to shape memory polyurethanes may significantly improve performance, offering a means to enhance the rubbery modulus and thus the restoring force[9] without changing the glass transition temperature.

The addition of 20 wt% Laponite to Elasthane induces an increase in the HDT of more than 100°C. This allows the nanocomposite to be used in higher temperature applications without risk of deformation. **Fig. 3c** and the movie in **Fig. S4** illustrate that under a constant load Elasthane films elongate by more than 100% and break at 120°C. In contrast, thin films containing 20 wt% Laponite exhibit no deformation at temperatures as high as 125°C. Furthermore, because the Laponite platelets are not organically modified, TGA shows that there is no risk of thermal degradation or decomposition at temperatures below 250°C (**Fig. S5**). Further investigation is necessary to determine what thermo-physical mechanism is responsible for the dramatic increase of the HDT when Laponite is added to the polyurethane—presumably both the percolative Laponite network and the enhancement in magnitude and intensity of the hard segment melting temperature which is observed in DSC data (**Fig. S3**) play a role. In general the melting temperature of a material increases if the intermolecular cohesive bonds holding the material together are strengthened and the intensity of a hard segment melting endotherm increases when the crystallite is more perfect[36]. Consequently, Laponite platelets must amplify a crystalline morphology with the hard micro-domains which accounts for the HS strengthening and the enhancement in melting endotherm intensity.

Microscopic images of the nanocomposite films taken under cross-polarized light like those depicted in **Fig. 4** and **Fig. S6** help to elucidate the influence of Laponite on the morphology of the polyurethane nanocomposite. The local mechanical properties and morphology of the ordered domains and the amorphous matrix are very different from one another. The birefringence and fractal-like shape of the ordered domains depicted in **Fig. 4b** and **Fig. S6** suggest a quenched phase transition process[44]. The scale of these ordered domains (20-100 μm) is much larger than the size of the hard micro-domains (20-175 nm)[30, 45]. The fraction of the image area occupied by these ordered-domains increases slightly with ϕ; however, this increase was close to the sample-to-sample variation with the same ϕ. As shown **Fig. 4a**, there is a rapid reduction in the fractional area of bright regions upon heating between 100°C and 120°C. This transition is similar to the local melting transition in thermotropic liquid-crystalline polymers. This long-range ordering is the result of an isotropic-nematic (I-N) transition of the hard micro-domains with and without the Laponite discs. Upon annealing the samples at 60°C, new, ordered, crystalline domains appeared within a few days time as shown in **Fig. 4c**. This re-crystallization behavior was not observed in the pure Elasthane sample even after annealing for many days. The re-crystallization behavior is again similar to that observed in thermotropic liquid-crystalline polymers in which mesogens are chemically attached to the polymer chains[46]. In our nanocomposites it appears that the Laponite platelets act as mesogens that are physically embedded in the hard micro-domains rather than chemically attached to the polymer chain. The amorphous matrix becomes birefringent after stretching via strain induced alignment and crystallization of the polymer chains during plastic deformation[47] and the ordered domains become disordered during stretching as evidenced by the darkening of the previously bright fields (**Figs. 4d-e**).

To verify that segment polarity and hydrophilicity determine the location of preferential reinforcement in either the soft or hard domain, thermoplastic polyurethane/Laponite nanocomposites were prepared using two custom-synthesized thermoplastic polyurethanes (TPUs) that differed in soft segment (SS) polarity and hydrophilicity[48]. If the SS attracts the charged clay discs, the Laponite preferentially segregates into the soft micro-domains. This significantly hinders SS mobility and therefore dramatically reduces the TPU extensibility[48]. Ultimately, the solvent exchange approach combined with the attraction of unmodified Laponite to polar and/or hydrophilic constituents afford material engineers the ability to select and control the location of nanoreinforcement and thus tailor the thermomechanical properties of polar block-copolymers such as polyurethanes and polyureas.

The new solvent exchange method outlined here allows block-copolymers with polar constituents, like thermoplastic polyurethanes, to be preferentially nanoreinforced with organic nanoparticles, like smectic clays. The efficacy of nanoreinforcement on thermomechanical properties hinges upon the close matching of characteristic length scale and the adhesion of the nanoparticles to the targeted polymer phase morphology. The hierarchical order induced by the addition of discotic Laponite platelets creates a percolated network that significantly stiffens and toughens the elastomer without reducing its extensibility. The use of block polarity in conjunction with this solvent exchange approach plus and processing techniques, such as electro-spinning, offers an avenue toward the development of high performance materials that rival natural materials.

Methods

Biomedical polyetherurethane, Elasthane^{TM} 80A was obtained from the Polymer Technology Group, Inc. (Berkeley, CA). Elasthane contains poly(tetramethylene oxide) (PTMO)

soft segments and 4,4'-methylene bisphenyl diisocyanate (MDI) hard segments chain extended with 1,4-butanediol (BDO). The hard-to-soft segment ratio of Elasthane 80A is 40:60 wt%, its molecular weight is 290,000 g/mol, and its density is 1.12 $g.cm^{-3}$ [12]. Laponite® RD, a synthetic smectic clay with a density of 2.65 $g.cm^{-3}$ [49] was obtained from Southern Clay Products, Inc. (Gonzales, TX). Dimethylacetamide (DMAc; B.P. 165°C) was obtained from Sigma Aldrich Co. (St. Louis, MO) and used as received. Laponite was dispersed in DMAc via a new solvent exchange procedure[33]. Solutions of Elasthane, Laponite, and DMAc were prepared from the resulting Laponite-DMAc dispersion. The Elasthane concentration in the solution was maintained at 1.4—1.6 wt%. Elasthane/Laponite nanocomposite films with 80-120 μm thicknesses were prepared in Teflon® containers (6 cm x 4 cm) by controlled evaporation of DMAc. The final Laponite concentration in the dry film was controlled by varying the Laponite concentration in the Laponite-Elasthane-DMAc solution. Note, for a discotic clay such as Laponite, the percolation threshold, $\tilde{\phi}_P$, can be approximated by dividing the random-close-packed hard sphere percolation volume fraction (~0.64) by the aspect-ratio, α, of the clay. The evaporation rate of DMAc was maintained by keeping the films in a closed 60°C oven with a 0.02 $m^3.hr^{-1}$ N_2 purge flow. A constant evaporation rate was maintained for all samples because the physical properties of the dry films were observed to depend on the evaporation rate. The mechanical properties of films prepared at higher evaporation rates proved repeatedly to be inferior.

The 10 wt% Laponite nanocomposite transmission electron microscope (TEM) sample was cut on a RMC MT-χ Cryo-capable Ultramicrotome with a diamond knife at -170°C and collected on 400 mesh copper grids. The TEM image was then obtained using a JEOL 200CX operated at 200 kV. The 4 wt% and 20 wt% Laponite nanocomposite TEM samples were

prepared in a JEOL JEM 9310 focused ion beam (FIB) instrument. These samples were first sputter-coated with ~200 nm of gold, and then a localized ~1 μm thick carbon protective film was deposited atop the selected area for lamella preparation. The samples were milled and polished in the FIB to give lamella measuring 10 μm by 10 μm by 80 nm. These samples were transferred to the copper grids using a micromanipulation system which consisted of a position-controlled polished glass rod that allowed for electrostatic pick-up of the lamella. These lamellae were observed in a JEOL 2010 containing a LaB6 filament and imaged using a Gatan digital camera.

Atomic force microscope (AFM) phase images of the nanocomposite samples (which were sandwiched between epoxy and cryo-microtomed) were taken in tapping mode using moderate force (Amplitude Set Point = 0.7 Volts, scale = 60°) and high force (0.3 Volts, 15°) on a Veeco Instruments Dimension 3100 AFM with the same Veeco NanoProbe (130 μm, 280-361 Hz). Note the magnified AFM phase image in Figure 1 was taken on the 10 wt% Laponite cryo-microtomed TEM sample at a different time with a different NanoProbe (amplitude set point = 0.85 Volts, scale = 20°).

Wide angle x-ray diffraction (WAXD) spectra from 10° to 80° were obtained using a Rigaku RU300 with an 18 kW rotating CuKα anode x-ray generator, a 185 mm diffractometer, and a scintillation counter, in the Bragg-Brettano mode. WAXD spectra from 2° to 38° were obtained using a Molecular Metrology small-angle X-ray scattering system with a custom-machined attachment so that WAXD *d*-spacings could be obtained.

Tensile tests were performed on thin film samples approximately 45 x 5 x 0.1 mm^3 and were carried out on an Zwick/Roell Z010 mechanical tester with a 500 N load cell at a constant crosshead speed of 100% initial length per minute. Differential scanning calorimetry (DSC)

measurements were performed on a TA Instruments Q1000 DSC at heating rate of 10°C.min^{-1}. Dynamic mechanical analysis (DMA) measurements were made at 1 Hz and at a heating rate of 3°C.min^{-1} using the TA Instruments Q800 DMA. A Carl Zeiss Axioskop 2MAT Polarizing Microscope was used to obtain birefringent images of the nanocomposites. The theoretical Laponite concentration in the films was verified by thermogravimetric analysis (TGA). TGA was performed under a 20 ml.min^{-1} N_2 purge at a heating rate of 10°C.min^{-1} with a Perkin Elmer TGA7. Multiple samples at each Laponite concentration were prepared and all DMA, DSC, and tensile tests were repeated a minimum of three times.

To demonstrate the thermomechanical integrity of these nanocomposites two films containing 0 and 20 wt% Laponite were held in improvised grips under a constant load equal to 1.08 N (initial stress of 1.75 MPa) and heated from 45°C to 125°C at ~1°C.min^{-1}. Photographs were captured as the experimental set-up underwent heating in an oven with a transparent window.

Acknowledgements

The authors acknowledge Dr. Steven Kooi, Dr. Mark Johnson, and Dr. Brian Pate for TEM sample preparation using the FIB, TEM examination of the FIB samples, and WAXD collection between 2° and 38°, respectively. This research was supported by the U.S. Army through the Institute for Soldier Nanotechnologies, under Contract DAAD-19-02-0002 with the U.S. Army Research Office. S.M. Liff was supported by a National Science Foundation Graduate Research Fellowship.

Figure captions:

FIGURE 1: **Structure of Elasthane 80A and Laponite dispersal within the polyurethane matrix. a,** Elasthane 80A is an elastomeric block-copolymer composed of MDI-BDO hard segments and PTMO soft segments. Hard segments (length 3-11 nm[19, 26]) phase segregate to form hard crystalline domains via hydrogen bonding[30]. The charged Laponite platelets (in orange) preferentially reinforce the polar hard domains. **b**, **c, & d,** Transmission electron micrographs (TEM) of nanocomposites containing 4, 10, and 20 wt% Laponite show fully exfoliated, uniformly dispersed and randomly oriented, Laponite platelets. Above the percolation concentration (ϕ_P = 5.9 wt%) jamming of Laponite platelets is observed. In the ϕ = 20 wt% micrograph some instances of intercalation are evident with a 2 nm spacing between platelets. **e**, Atomic Force Microscope (AFM) phase image of the surface of the same ϕ = 10 wt% TEM sample shows stiff, single Laponite particles (bright fields) cut at different orientations. Image width is 383 nm. **f**, Wide angle x-ray diffraction (WAXD) spectra of nanocomposites containing 0, 4, 10 and 20 wt% Laponite and of Laponite powder[50] (from bottom to top). The d001 spacing of Laponite is 1.28 nm (2θ = 6.92°). This diffraction shoulder is observed in the ϕ = 10 and 20 wt% samples with increased intensity at a spacing of 2.02 nm (2θ = 4.36°), indicating the instances of Laponite intercalation increase as ϕ surpasses ϕ_p. The incomplete exfoliation at $\phi \geq \phi_p$ is a consequence of the increased Laponite volume fraction and the slow solvent evaporation which result in weak particle-particle interactions[24, 30] (See Fig S1). The peak at 2θ = 20° corresponds to hard segment crystallites with lattice spacing of 4.43 Å[30, 50].

Figure 1

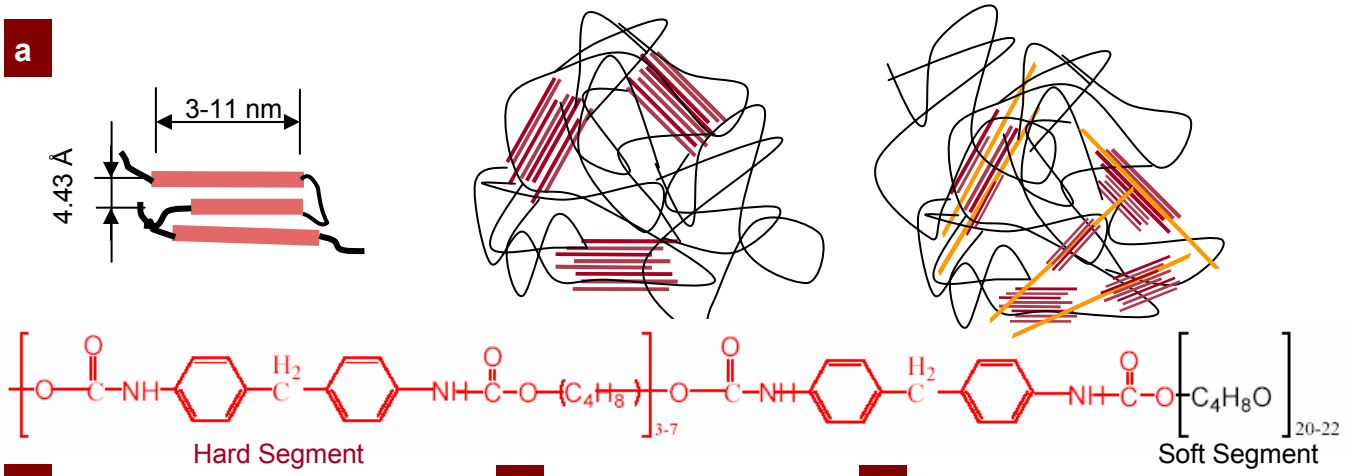
a
3-11 nm
4.43 Å
Hard Segment
Soft Segment
3-7
20-22

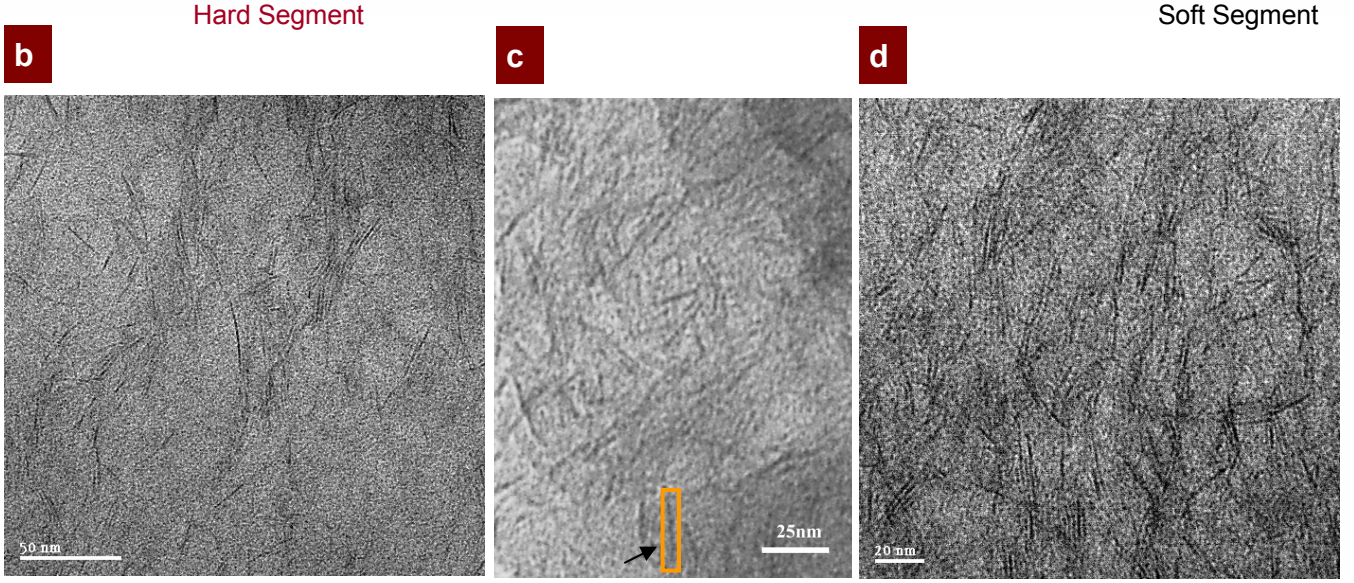
b
c
d
50 nm
25nm
20 nm

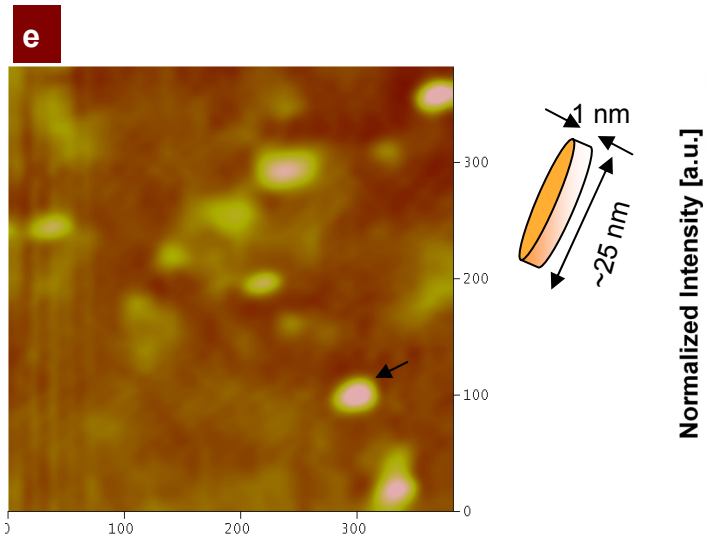
e
300
200
100
0
100
200
300

1 nm
~25 nm

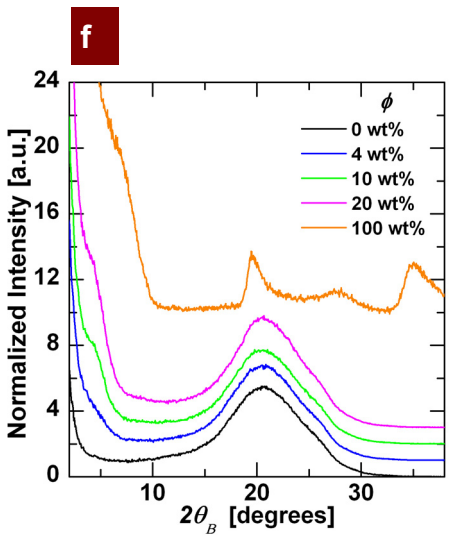
f
Normalized Intensity [a.u.]
2θB [degrees]
ϕ
0 wt%
4 wt%
10 wt%
20 wt%
100 wt%
0
4
8
12
16
20
24
10
20
30

FIGURE 2: **Impact of Laponite concentration on the mechanical properties of Elasthane.** **a,** Representative engineering stress-strain (σ–ε) curves of thin film nanocomposites containing between 0 and 20 wt% Laponite. **b**, Initial elastic modulus, E, increases with increasing Laponite concentration, ϕ. For $\phi < \phi_P$ the prediction of Guth's model (Equation 1; red line) is in excellent agreement with experimental values. The agreement of Guth's model using $\alpha = 25$ further demonstrates that the Laponite is completely exfoliated. For $\phi > \phi_P$ the sharp increase in E follows the typical scaling (Equation 2; blue dashed-line) of jammed systems[38]. **c**, Toughness, $U_{0.3}$, (defined as the area under the σ-ε curve up to $\varepsilon = 0.3$) increases quadratically with ϕ (Equation 3; blue line), so $U_{0.3}$ of a nanocomposite containing 20 wt% Laponite is 4.25 times greater than that of pure Elasthane.

Figure 2

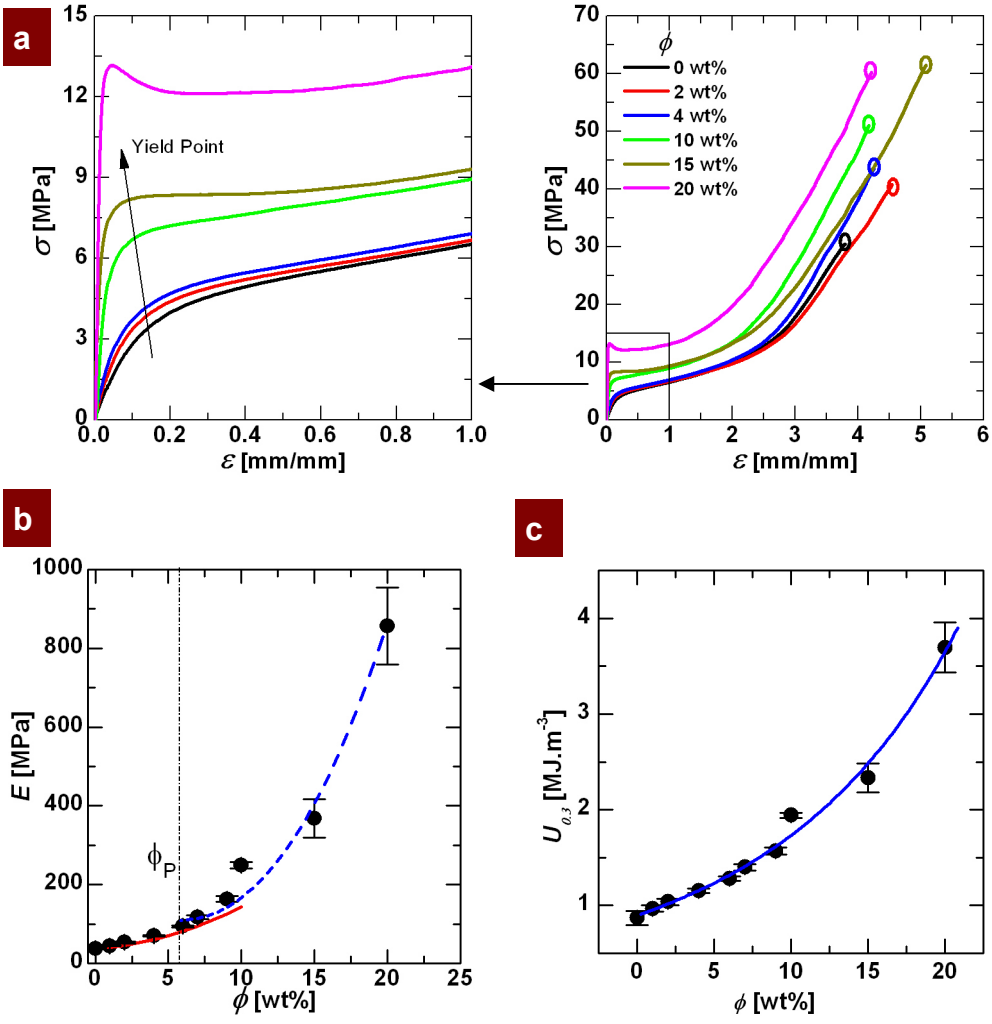
a
Yield Point
σ [MPa]
ε [mm/mm]
ϕ
0 wt%
2 wt%
4 wt%
10 wt%
15 wt%
20 wt%
b
E [MPa]
ϕP
ϕ [wt%]
c
U0.3 [MJ.m-3]
ϕ [wt%]

FIGURE 3: **Impact of Laponite concentration on the thermomechanical properties of Elasthane. a,** The ratio of the flexural storage modulus to the loss modulus at various temperatures, or *tan(δ)* curve, for nanocomposites containing between 0 and 20 wt% Laponite measured by Dynamic Mechanical Analysis (DMA). The soft segment glass transition temperature ($T_{g,SS}$), indicated by the peak at –25°C in the curve, does not change significantly with increasing ϕ. A new peak at 29°C observed in nanocomposites with $\phi \geq 15$ wt% suggests the onset of crystallization in soft domains. Equivalent transitions also appear in the DSC data shown in supporting material Fig. S3. **b**, Increasing the concentration of Laponite in the nanocomposite does not significantly change the magnitude of the flexural storage modulus (E') prior to the onset of the soft segment glass transition at –50°C. Above this temperature the magnitude of E' increases significantly with ϕ. The steep fall in E' at high temperatures ($T > 130$°C) is due to the softening of the Elasthane caused by the melting of the hard domains. The heat distortion temperatures (HDT), which may be defined as the temperature at which $E' = 8$ MPa (see ISO 75—method C) for nanocomposites with $\phi = 0$, 2, 4, 8, 10, and 20 wt% are 101,111, 134, 161, >160, >200°C, respectively. The exact values of the HDT for nanocomposites with $\phi > 10$ wt% could not be measured due to instrument limitations. **c,** Demonstration of the mechanical enhancement of Elasthane at high temperature by the addition of Laponite (Fig. S4). The pure Elasthane exhibits little resistance to heat distortion, deforming significantly with increase in temperature, reaching the maximum allowable extension at 95°C, and finally breaking at 120°C. The nanocomposite containing 20 wt% Laponite resists heat distortion and does not show visually any deformation upon heating; however, at 125°C the grips slipped from the sample. Length of scale bar: 46 mm.

Figure 3

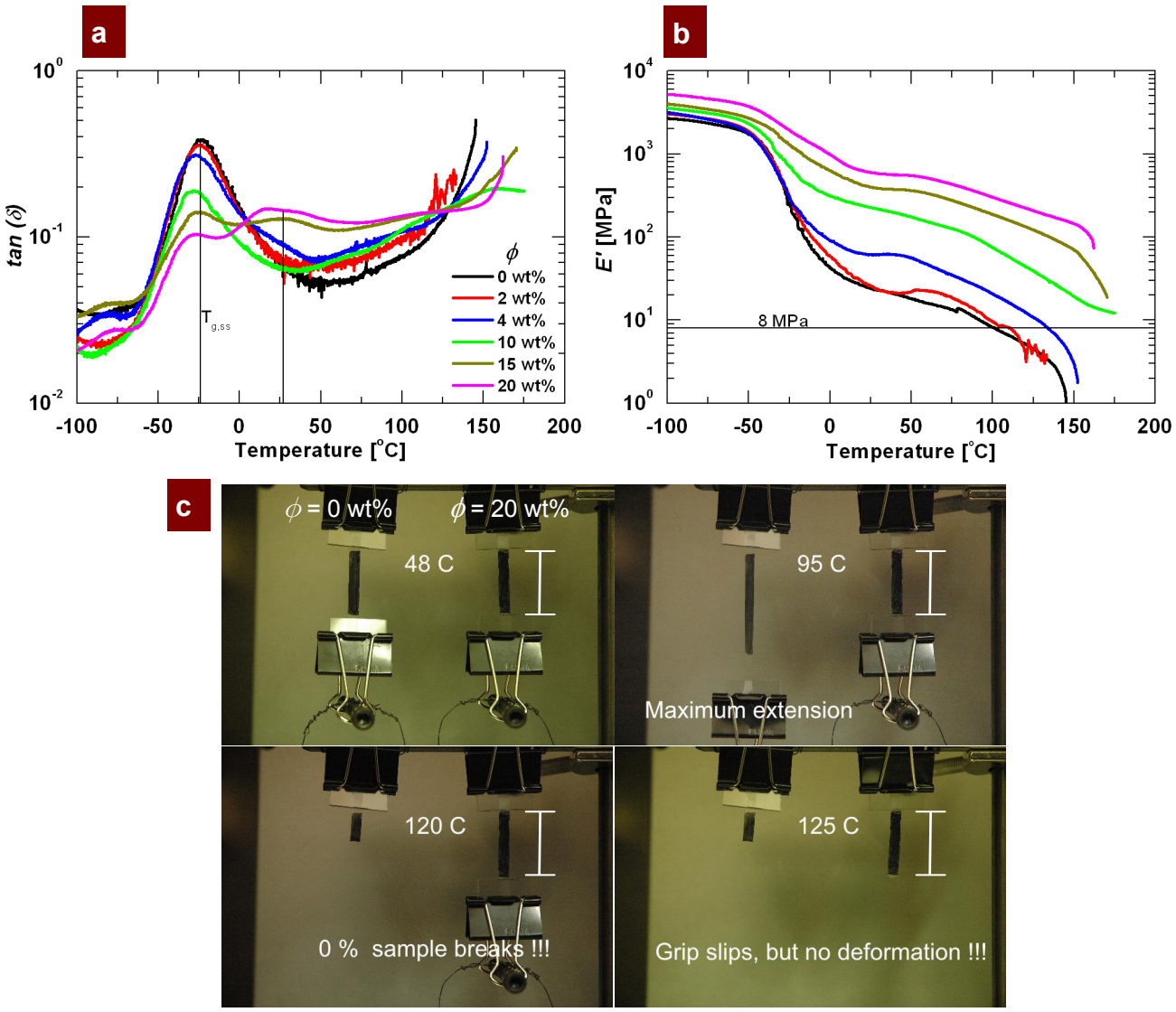
a
b
c
tan (δ)
E' [MPa]
Temperature [°C]
T g,ss
ϕ
0 wt%
2 wt%
4 wt%
10 wt%
15 wt%
20 wt%
8 MPa
ϕ = 0 wt%
ϕ = 20 wt%
48 C
95 C
Maximum extension
120 C
125 C
0 % sample breaks !!!
Grip slips, but no deformation !!!

FIGURE 4: **Evidence of long range order or crystallization in the nanocomposites is apparent in images obtained with a cross-polarized microscope. a**, Bright crystalline domains in a nanocomposite containing 10 wt% Laponite are due to the long-range ordering of the Elasthane hard domains. **b,** The fractal-like shape of the crystalline domains is typical of a quenched phase transformation. Upon heating, the bright domains undergo a nematic-isotropic transition between 100 and 120°C. **c**, Crystalline domains reappeared upon annealing the sample for a few days at 60°C. **d,** Birefringent image of a nanocomposite containing 10 wt% Laponite after tensile testing. The unstretched region on the left side of the grip line exhibits these same bright domains. Upon stretching the amorphous matrix becomes birefringent as a result of strain induced alignment and crystallization of the polymer chains during plastic deformation[47]. **e**, The ordered domains become disordered upon stretching as evidenced by the darkening of these previously bright domains. Similar birefringence results are also obtained in pure Elasthane films. Image widths are as follow: (a) 2700 μm, (b) 337 μm, (c) 270 μm, (d) 2700 μm, and (e) 337 μm.

Figure 4

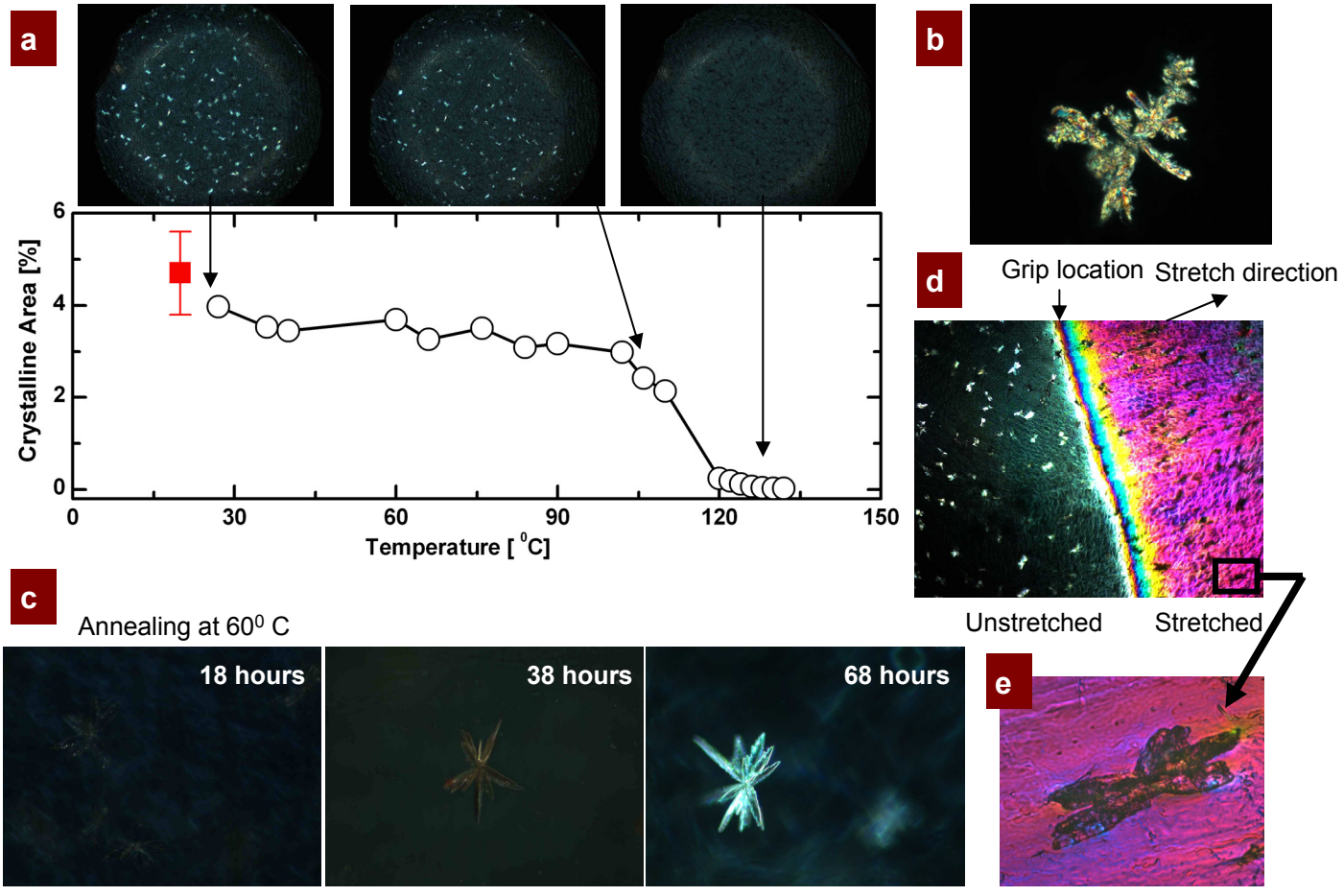
a
b
d
Grip location
Stretch direction
Crystalline Area [%]
Temperature [^{0}C]
Unstretched
Stretched
c
Annealing at 60^0 C
18 hours
38 hours
68 hours
e

Supplementary Figure Captions:

FIGURE S1: **Laponite dispersal within the polyurethane matrix via WAXD. a,** Spectra from 2θ = 10° to 80° of nanocomposites containing 0, 4, 10 and 20 wt% Laponite and of Laponite powder[50] (from bottom to top), using a different diffraction instrument and different nanocomposite samples (Methods). Because Laponite has only weak reflections due to imperfect platelet registration and its small size, the broad diffraction halo of the Elasthane would mask the peak at 2θ = 19.5°. Although no large angle peaks are observed in the ϕ < 20 wt% samples, the Laponite peak at 27.4° is observed in the ϕ = 20 wt% spectra shifted to 26.4°. At this high Laponite volume fraction, particle-particle interactions over the long time allowed for slow solvent removal cause the platelets to re-aggregate in an intercalated state. Note, the WAXD spectra of numerous nanocomposite samples at various Laponite concentration have been examined using numerous WAXD instruments, including the G1 beamline at the Cornell high-energy synchrotron source (CHESS)[S1] and are broadly consistent. In numerous instances at Laponite concentrations above the percolation threshold, but below 20 wt% ($\phi_P \leq \phi \leq$ 20 wt%), nanocomposite spectra did not exhibit any peaks or shoulders corresponding to the pure Laponite spectra.

Figure S1

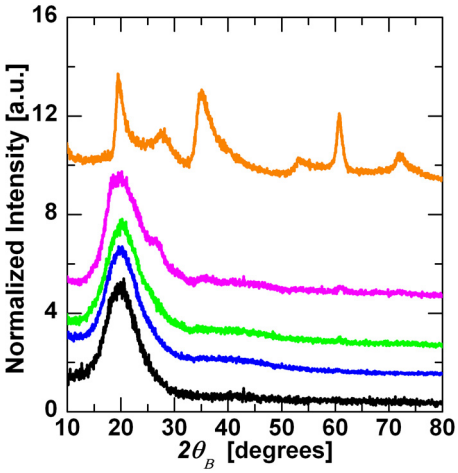
Normalized Intensity [a.u.]
16
12
8
4
0
10
20
30
40
50
60
70
80
2θ_B [degrees]

FIGURE S2: **Hard and soft micro-domain distribution in nanocomposites containing 0, 4, 10, and 20 wt % Laponite as observed via AFM phase imaging.** The same areal extent on each nanocomposite was imaged with moderate tapping force (amplitude set point = 0.7 Volts, scale = 60°, left) and with high tapping force (0.3 Volts, 15°, right). The bright regions correspond to material of high modulus within the softer matrix material. AFM phase imaging is often used to distinguish hard and soft micro-domains in polyurethanes because there is often insufficient contrast in electron density between phases and effective staining procedures prove too time-consuming to make TEM effective [45]. Extensive analysis of AFM images showed repeatedly that as more of the high modulus Laponite is added the bright areas brighten and grow in size, indicating that the Laponite imposes a change in hard domain texture. As the Laponite concentration increases the discrete hard micro-domains become interconnected, and in conjunction with the Laponite this accounts for the increased initial modulus and distinct yield point. The bright white regions on the left, which correspond to regions occupied by the very highest modulus moieties on the right, are believed to be a combination of Laponite and hard polyurethane micro-domains at the surface. With AFM it is difficult to distinguish the Laponite platelets from the hard polyurethane micro-domains due to the preferential association of the Laponite and the irregular shape formation of the hard micro-domains. The hard micro-domains in the bulk Elasthane are unlike the fibrillar hard micro-domain structures observed in AFM phase images of piperazine-butanediol-poly(tetramethylene oxide) and hexamethylene diisocyanate-butanediol-poly(ethylene oxide)-poly(propylene oxide) poly(ethylene oxide) polyurethanes[45, S2] or the large, spherical hard micro-domain structures observed in methylene-bis(cyclohexyl isocyanate)-butanediol-poly(propylene glycol)[S3]. The soft domains observed in the present study do not form irregular spherical soft micro-domains which are observed in AFM

phase images of bisphenyl methylene diisocyanate-dendrimer-poly(tetramethylene oxide) polyurethanes[S4]. Instead the hard micro-domain morphology observed in these images is similar to the morphology observed by Eisenbach et al. via element-specific electron-microscopy and by McLean and Sauer using tapping-mode AFM in polyurethanes of similar composition[26, S5].

Figure S2

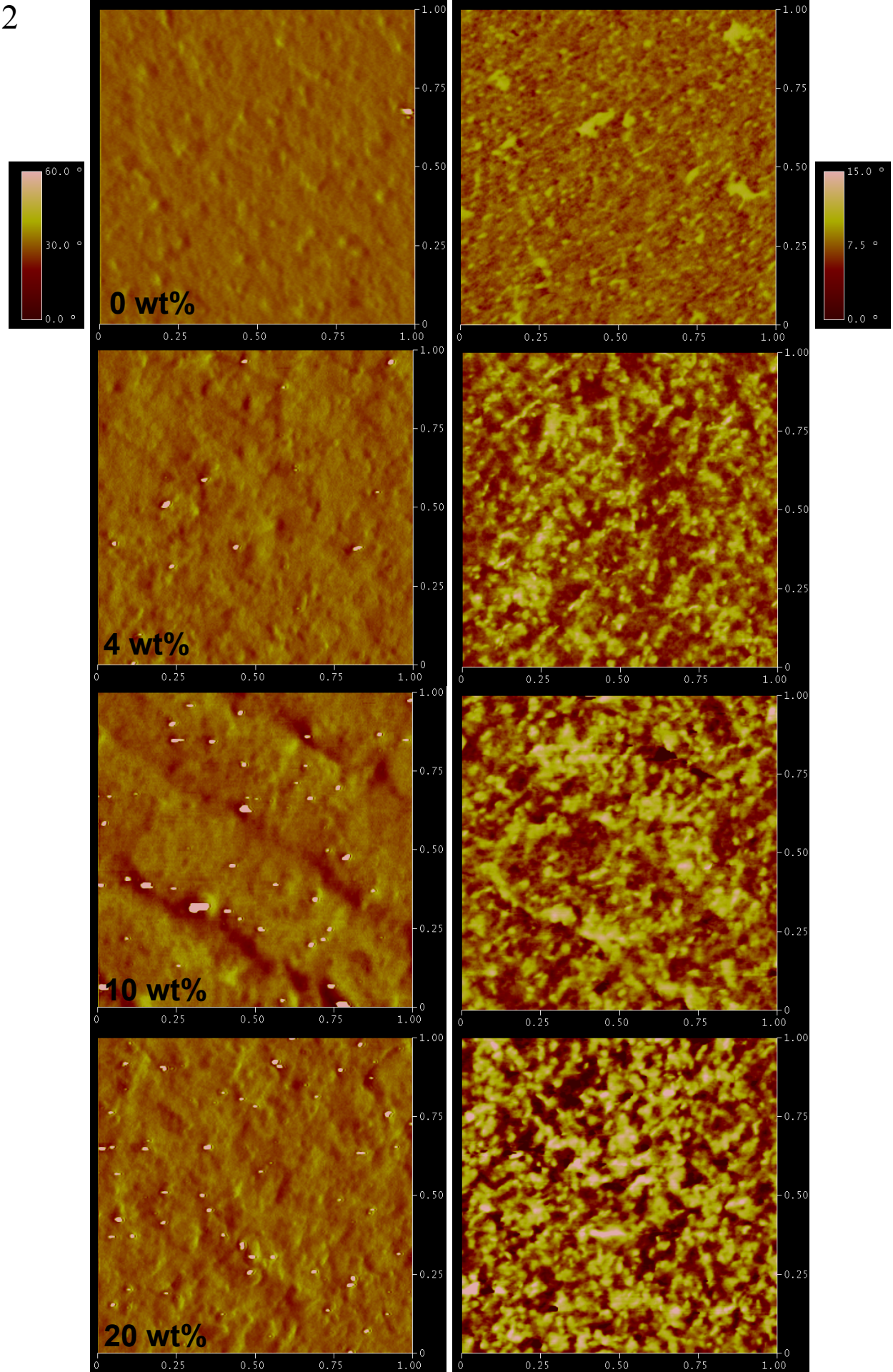

FIGURE S3: **DSC of the nanocomposites containing 0, 4, 10, and 20 wt% Laponite**. **a**, DSC curves during the first heating and cooling cycle show both reversible and irreversible transitions. **b**, Subsequent heating and cooling cycles show reversible transitions. Pure Elasthane exhibits a reversible hard segment melting endotherm and crystallization exotherm at 150°C and 77°C, respectively, which agree with the values reported in literature[19, 30]. With increasing Laponite concentration, ϕ, this peak reduces in intensity, and finally disappears in nanocomposites with $\phi > 6$ wt%. This behavior is attributed to the restricted motion of the hard segments due to the disruption by and jamming of Laponite above the percolation concentration ($\phi_P = 5.9$ wt%). Furthermore, an irreversible melting peak observed in the first heating cycle near 227°C is not observed in the samples during the subsequent heating cycles. The increased intensity of this peak is attributed to interactions between the hard segment and the Laponite since the peak intensity increases with ϕ. The origin of the broad dip in the first heating cycle near 150°C observed in the 10 wt% and 20 wt% nanocomposite thermograms cannot be resolved but may result from soft segment and Laponite interactions. The glass transition temperature of the soft segment, $T_{g,SS}$ at -41°C does not change, but nanocomposites with $\phi \geq 15$ wt% exhibit an interphase reversible melting/crystallization peak at 10°C and –25°C during the heating and cooling cycles, respectively. Similar results are observed in DMA measurements (Fig. 3a).

Figure S3

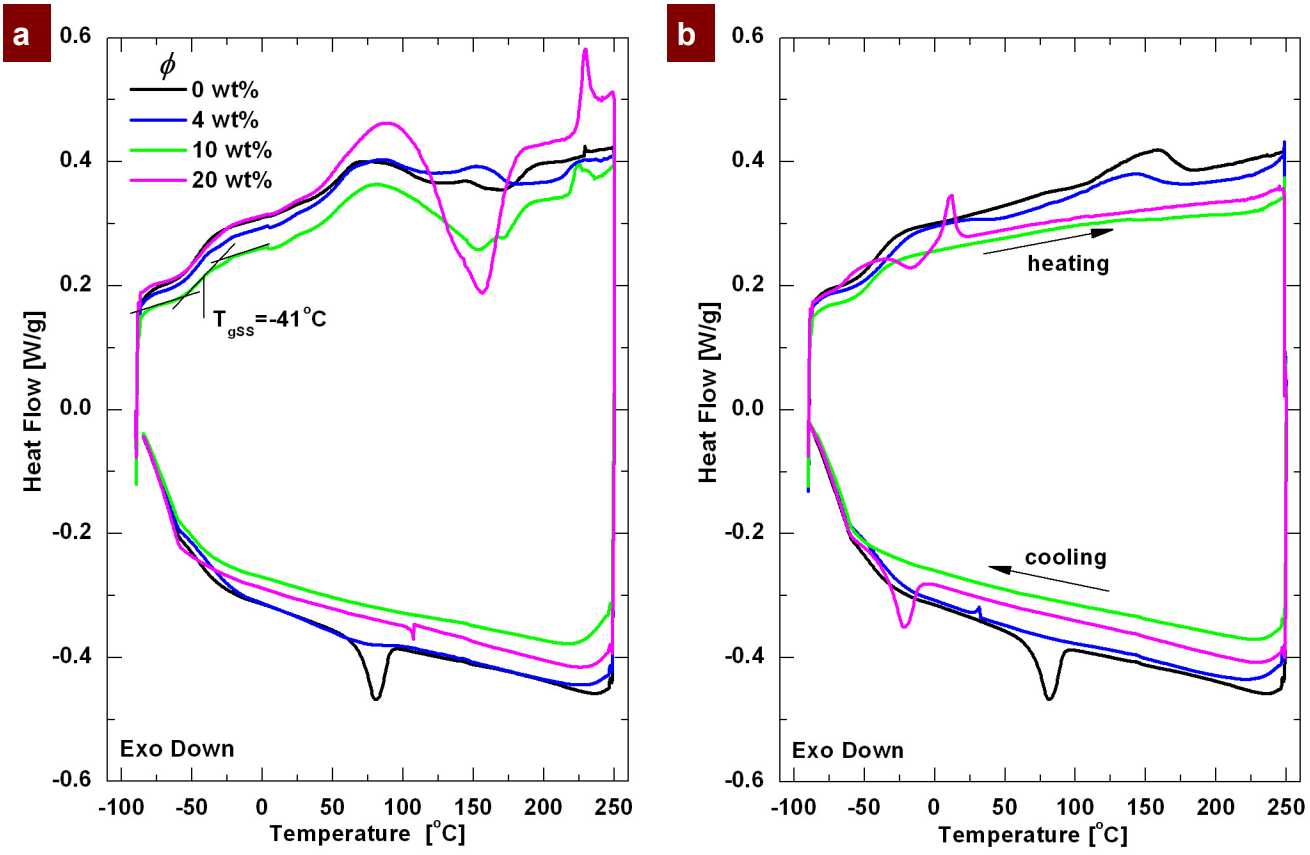
a
b
ϕ
0 wt%
4 wt%
10 wt%
20 wt%
T_gss=-41°C
heating
cooling
Exo Down
Heat Flow [W/g]
Temperature [°C]
0.6
0.4
0.2
0.0
-0.2
-0.4
-0.6
-100
-50
0
50
100
150
200
250

FIGURE S4: **Movie displaying thermal creep of nanocomposite films containing 0 and 20 wt% Laponite when a constant load equal to 1.08 N is applied.** The pure Elasthane deforms significantly, increasing its length by 100% at 95°C, and breaks at 120°C. Meanwhile the nanocomposite containing 20 wt% Laponite does not measurably deform at all. However, at 125°C the improvised grip holding the constant load slips off the sample.

Figure S4

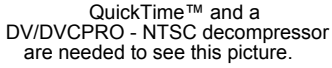
QuickTime™ and a
DV/DVCPRO - NTSC decompressor
are needed to see this picture.

FIGURE S5: **Laponite concentration and impact on thermal degradation. a**, Thermogravimetric analysis (TGA) of nanocomposites containing 0 to 20 wt% Laponite. The rapid loss in weight is due to the degradation of the Elasthane. **b**, Residue weight fraction at 1000°C of the various nanocomposites is nearly equal to the weight fraction of Laponite blended with Elasthane in each case. This is demonstrated by the agreement of the experimental data with a line of slope one. Increasing Laponite fraction decreases the thermal degradation temperature which is defined as the temperature at which the sample weight decreases by 5%.

Figure S5

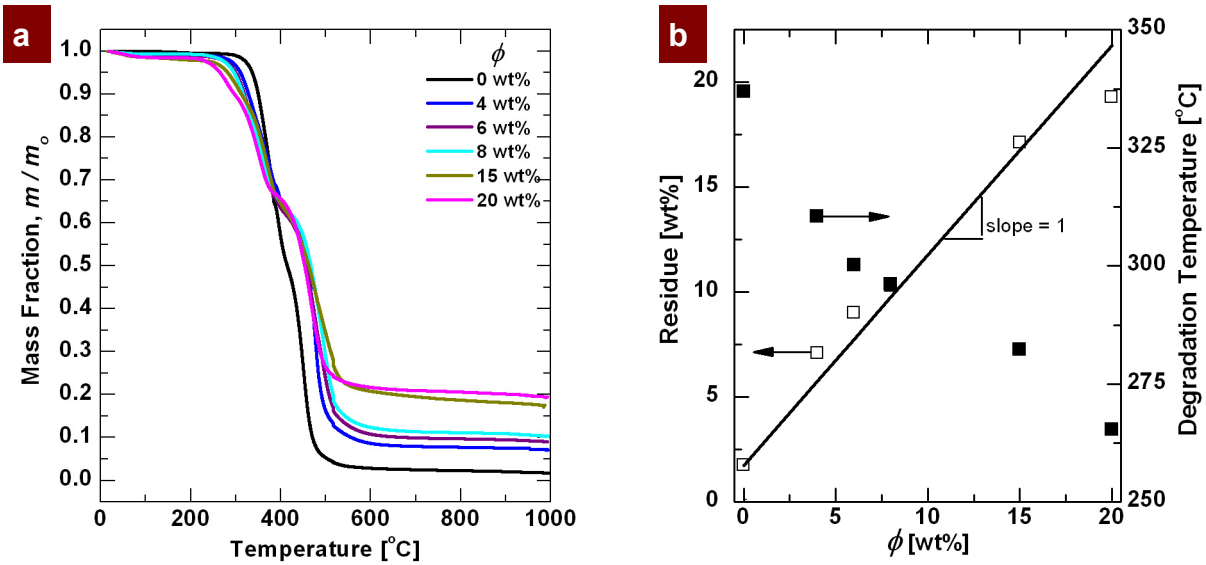
a
Mass Fraction, m / m_o
Temperature [°C]
ϕ
0 wt%
4 wt%
6 wt%
8 wt%
15 wt%
20 wt%
b
Residue [wt%]
Degradation Temperature [°C]
ϕ [wt%]
slope = 1

FIGURE S6: **Polarized optical microscopy images of the ordered, fractal-like domains in various nanocomposite films exhibit birefringence.** Image width is as follows: (a) 270 μm, (b) 135 μm, (c) 675 μm, (d) 270 μm, (e) 675 μm, (f) 270 μm, (g) 135μm, and (h) 337 μm.

Figure S6

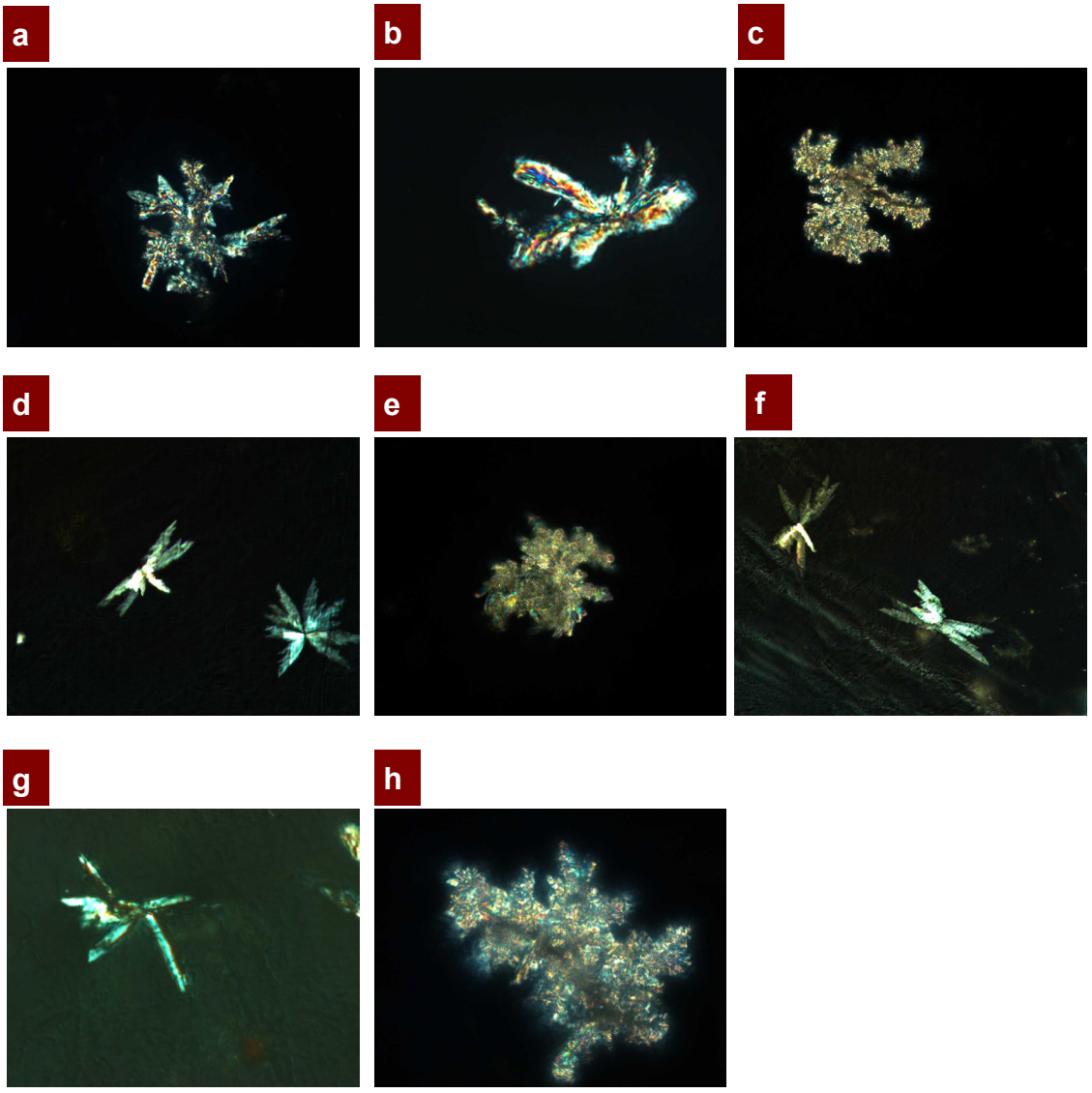

References

1. Knight, D. P. & Vollrath, F. Biological liquid crystal elastomers. *Philosophical Transactions of the Royal Society of London Series B-Biological Sciences*. **357**, 155-163 (2002).
2. Vollrath, F. & Knight, D. P. Liquid crystalline spinning of spider silk. *Nature*. **410**, 541-548 (2001).
3. Termonia, Y. Molecular Modeling of Spider Silk Elasticity. *Macromolecules*. **27**, 7378-7381 (1994).
4. Simmons, A. H., Michal, C. A. & Jelinski, L. W. Molecular orientation and two-component nature of the crystalline fraction of spider dragline silk. *Science*. **271**, 84-87 (1996).
5. van Beek, J. D. et al. Solid-state NMR determination of the secondary structure of Samia cynthia ricini silk. *Nature*. **405**, 1077-1079 (2000).
6. Gao, H. J., Ji, B. H., Jager, I. L., Arzt, E. & Fratzl, P. Materials become insensitive to flaws at nanoscale: Lessons from nature. *Proceedings of the National Academy of Sciences of the United States of America*. **100**, 5597-5600 (2003).
7. Smith, B. L. et al. Molecular mechanistic origin of the toughness of natural adhesives, fibres and composites. *Nature*. **399**, 761-763 (1999).
8. Gosline, J., Guerette, P., Ortlepp, C. & Savage, K. The mechanical design of spider silks: from fibroin sequence to mechanical function. *J Exp Biol*. **202**, 3295-3303 (1999).
9. Koerner, H., Price, G., Pearce, N. A., Alexander, M. & Vaia, R. A. Remotely actuated polymer nanocomposites - stress-recovery of carbon-nanotube-filled thermoplastic elastomers. *Nature Materials*. **3**, 115-120 (2004).

10. Vaia, R. A. & Wagner, H. D. Framework for nanocomposites. *Materials Today*. **7**, 32-37 (2004).

11. Szycher, M. *Szycher's Handbook of Polyurethanes* (CRC Press, Boca Raton, 1999).

12. Wiggins, M. J., MacEwan, M., Anderson, J. M. & Hiltner, A. Effect of soft-segment chemistry on polyurethane biostability during in vitro fatigue loading. *Journal Of Biomedical Materials Research Part A*. **68A**, 668-683 (2004).

13. Finnigan, B. et al. Segmented polyurethane nanocomposites: Impact of controlled particle size nanofillers on the morphological response to uniaxial deformation. *Macromolecules*. **38**, 7386-7396 (2005).

14. Yeh, F., Hsiao, B. S., Sauer, B. B., Michel, S. & Siesler, H. W. In-situ studies of structure development during deformation of a segmented poly(urethane-urea) elastomer. *Macromolecules*. **36**, 1940-1954 (2003).

15. Kim, H. D., Lee, T. J., Huh, J. H. & Lee, D. J. Preparation and properties of segmented thermoplastic polyurethane elastomers with two different soft segments. *Journal of Applied Polymer Science*. **73**, 345-352 (1999).

16. Nair, B. R., Gregoriou, V. G. & Hammond, P. T. FT-IR studies of side chain liquid crystalline thermoplastic elastomers. *Polymer*. **41**, 2961-2970 (2000).

17. Yeganeh, H. & Shamekhi, M. A. Poly(urethane-imide-imide), a new generation of thermoplastic polyurethane elastomers with enhanced thermal stability. *Polymer*. **45**, 359-365 (2004).

18. Stanford, J. L., Still, R. H. & Wilkinson, A. N. Effects of soft-segment prepolymer functionality on structure - property relations in RIM copolyurethanes. *Polymer*. **44**, 3985-3994 (2003).

19. Martin, D. J., Meijs, G. F., Gunatillake, P. A., Yozghatlian, S. P. & Renwick, G. M. The influence of composition ratio on the morphology of biomedical polyurethanes. *Journal of Applied Polymer Science*. **71**, 937-952 (1999).

20. Ryan, A. J., Stanford, J. L. & Birch, A. J. Copolyureas formed by reaction injection moulding: correlations between chemical structure, thermal properties and microphase separation. *Polymer*. **34**, 4874-4881 (1993).

21. Lee, D. K. & Tsai, H. B. Properties of segmented polyurethanes derived from different diisocyanates. *Journal of Applied Polymer Science*. **75**, 167-174 (2000).

22. Knight, D. P., Knight, M. M. & Vollrath, F. Beta transition and stress-induced phase separation in the spinning of spider dragline silk. *International Journal Of Biological Macromolecules*. **27**, 205-210 (2000).

23. Porter, D., Vollrath, F. & Shao, Z. Predicting the mechanical properties of spider silk as a model nanostructured polymer. *European Physical Journal E*. **16**, 199-206 (2005).

24. Sinha Ray, S. & Okamoto, M. Polymer/layered silicate nanocomposites: a review from preparation to processing. *Progress in Polymer Science*. **28**, 1539-1641 (2003).

25. Thostenson, E. T., Li, C. & Chou, T.-W. Nanocomposites in context. *Composites Science and Technology*. **65**, 491-516 (2005).

26. Eisenbach, C. D., Ribbe, A. & Gunter, C. Morphological-Studies Of Model Polyurethane Elastomers By Element-Specific Electron-Microscopy. *Macromolecular Rapid Communications*. **15**, 395-403 (1994).

27. Alexandre, M. & Dubois, P. Polymer-layered silicate nanocomposites: preparation, properties and uses of a new class of materials. *Materials Science and Engineering: R: Reports*. **28**, 1-63 (2000).

28. Njuguna, J. & Pielichowski, K. Polymer nanocomposites for aerospace applications: Fabrication. *Advanced Engineering Materials*. **6**, 193-203 (2004).

29. Burgentzle, D., Duchet, J., Gerard, J. F., Jupin, A. & Fillon, B. Solvent-based nanocomposite coatings: I. Dispersion of organophilic montmorillonite in organic solvents. *Journal of Colloid and Interface Science*. **278**, 26-39 (2004).

30. Finnigan, B., Martin, D., Halley, P., Truss, R. & Campbell, K. Morphology and properties of thermoplastic polyurethane nanocomposites incorporating hydrophilic layered silicates. *Polymer*. **45**, 2249-2260 (2004).

31. Dai, X. H. et al. Study on structure and orientation action of polyurethane nanocomposites. *Macromolecules*. **37**, 5615-5623 (2004).

32. Rhoney, I., Brown, S., Hudson, N. E. & Pethrick, R. A. Influence of processing method on the exfoliation process for organically modified clay systems. I. Polyurethanes. *Journal of Applied Polymer Science*. **91**, 1335-1343 (2004).

33. Kumar, N., Liff, S. M. & McKinley, G. H. Method to disperse and exfoliate nanoparticles. U.S. Patent Application 11/253,219 (Filed October 18, 2005).

34. Lee, H. S., Yoo, S. R. & Seo, S. W. Domain and segmental deformation behavior of thermoplastic elastomers using synchrotron SAXS and FTIR methods. *Journal of Polymer Science Part B-Polymer Physics*. **37**, 3233-3245 (1999).

35. Wang, C. B. & Cooper, S. L. Morphology and properties of segmented polyether polyurethaneureas. *Macromolecules*. **16**, 775-786 (1983).

36. Young, R. J. & Lovell, P. A. *Introduction to Polymers* (Chapman and Hall, London, 1991).

37. Guth, E. Theory of filler reinforcement. *Journal of Applied Physics*. **16**, 20-25 (1945).

38. Trappe, V., Prasad, V., Cipelletti, L., Segre, P. N. & Weitz, D. A. Jamming phase diagram for attractive particles. *Nature*. **411**, 772-775 (2001).

39. O'Hern, C. S., Silbert, L. E., Liu, A. J. & Nagel, S. R. Jamming at zero temperature and zero applied stress: The epitome of disorder. *Physical Review E (Statistical, Nonlinear, and Soft Matter Physics)*. **68**, 011306 (2003).

40. Petrovic, Z. S., Javni, I., Waddon, A. & Banhegyi, G. Structure and properties of polyurethane-silica nanocomposites. *Journal of Applied Polymer Science*. **76**, 133-151 (2000).

41. Frogley, M. D., Ravich, D. & Wagner, H. D. Mechanical properties of carbon nanoparticle-reinforced elastomers. *Composites Science and Technology*. **63**, 1647-1654 (2003).

42. Zhang, T. et al. Synthesis, properties of fullerene-containing polyurethane-urea and its optical limiting absorption. *Polymer*. **44**, 2647-2654 (2003).

43. Tang, Z. Y., Kotov, N. A., Magonov, S. & Ozturk, B. Nanostructured artificial nacre. *Nature Materials*. **2**, 413-U418 (2003).

44. Dierking, I. Liquid crystalline fractals: dilatation invariant growth structures in the phase ordering process of 'banana-phases'. *Liquid Crystals Today*. **12**, 1-10 (2003).

45. Aneja, A. & Wilkes, G. L. A systematic series of 'model' PTMO based segmented polyurethanes reinvestigated using atomic force microscopy. *Polymer*. **44**, 7221-7228 (2003).

46. Acierno, D. et al. Synthesis and characterisation of a nematic homo-polyurethane. *Polymer*. **44**, 4949-4958 (2003).

47. Kojio, K., Nakamura, S. & Furukawa, M. Effect of side methyl groups of polymer glycol on elongation-induced crystallization behavior of polyurethane elastomers. *Polymer*. **45**, 8147-8152 (2004).

48. Korley, L. T. J., Liff, S. M., Kumar, N., McKinley, G. H. & Hammond, P. T. Preferential association of segment blocks in polyurethane nanocomposites. *Macromolecules*. **ASAP Article**, (2006).

49. Grillo, I., Levitz, P. & Zemb, T. Insertion of small anisotropic clay particles in swollen lamellar or sponge phases of nonionic surfactant. *European Physical Journal E*. **5**, 377-386 (2001).

50. Malwitz, M. M., Lin-Gibson, S., Hobbie, E. K., Butler, P. D. & Schmidt, G. Orientation of platelets in multilayered nanocomposite polymer films. *Journal of Polymer Science Part B-Polymer Physics*. **41**, 3237-3248 (2003).

Supplementary References:

S1. http://www.chess.cornell.edu/gline/index.htm

S2. Korley, L.T.J., Pate, B.D., Thomas, E.L. & Hammond, P.T. Effect of the degree of soft and hard segment ordering on the morphology and mechanical behavior of semicrystalline segmented polyurethanes. *Polymer* **47**, 3073-3082 (2006).

S3. Song, M., Xia, H.S., Yao, K.J. & Hourston, D.J. A study of phase morphology and surface properties of polyurethane/organoclay nanocomposite. *European Polymer Journal.* **41**, 259-266 (2005).

S4. Chen, C.P. et al. Polyurethane elastomers through multi-hydrogen-bonded association of dendritic structures. *Polymer.* **46**, 11849-11857 (2005).

S5. McLean, R.S. & Sauer, B.B. Tapping-mode AFM studies using phase detection for resolution of nanophases in segmented polyurethanes and other block copolymers. *Macromolecules.* **30**, 8314-8317 (1997).